Carrier mobility enhancement on the H-terminated diamond surface

Jinlong Liu[1], Hua Yu[1], Siwu Shao[1], Juping Tu[1], Xiaohua Zhu[1], Xiaolu Yuan[1], Junjun Wei[1], Liangxian Chen[1], Haitao Ye[2], Chengming Li[1]*

[1]Institute for Advanced Materials and Technology, University of Science and Technology Beijing, Beijing 100083, China;

[2]Department of Engineering, University of Leicester, Leicester, LE1 7RH, UK

Abstract: The surface conductivity on the H-terminated diamond is still an interesting topic in the field of diamond electronics. Until now, the carrier mobility in the conductive channel has been limited to below 200cm^2/Vs due to the various surface scattering mechanisms. In this paper, a high mobility conductive channel on the H-terminated diamond surface was reported. Firstly, the high quality diamond films were deposited on the commercial CVD diamond substrates. After polishing, the H-termination was obtained by hydrogen plasma treatment. The surface morphology of the H-terminated diamond was observed by atomic force microscope(AFM) and scanning electron microscope(SEM). The crystal quality on the diamond surface was characterized by Raman spectroscopy. The impurities in the crystals were tested by photoluminescence spectroscopy. The surface conductivity of H-terminated diamond was monitored comprehensively by Hall test. It can be found that the sheet resistance decreases much and the carrier mobility increases dramatically after the hydrogen plasma treatment and mechanical cleaning. The maximum mobility value is up to 365cm^2/Vs with carrier density of 2.9 $\times 10^{12}$ cm^{-2}, which is the highest value reported. Raman spectra of diamond surface show that a peak appears at 1121.4cm^{-2} after the hydrogen plasma treatment, which corresponds to the nanocrystal diamond or carbon clusters of sp3 bonded material. The corresponding mobility enhancement mechanism on the H-terminated diamond surface was proposed.

Keywords: Diamond; H-termination; surface conductivity; carrier mobility enhancement; sp3 cluster.

Introduction

With the development of diamond preparation techniques, diamond is no longer limited to the applications in the traditional knife tools, heat dissipation devices and optical windows, and expected to be used as various semiconductor devices. Diamond has become one of the most promising wide band-gap semiconductor materials due to its extremely high thermal conductivity, high breakdown electric field, high power capacity, low dielectric constant, high saturation carrier velocity and mobility, etc[1-3].

One of the most interesting features is that the H-terminated diamond shows a negative electron

affinity and p-type surface conductivity like a quasi two-dimensional hole gas due to the transfer doping effect[4-6]. The surface conductivity is usually 10^{-4}-10^{-6} S/□, accompanying with the carrier density of 10^{11}-10^{14}cm^{-2} and mobility of 30-200 cm^2/Vs in the conductive channel[7-8]. The surface conductivity of H-terminated diamond will be affected by the adsorbates. For example, the surface conduction behavior will be controlled by the electrochemical system when exposed in the air[4]. To improve the stability of the conductive channel on H-terminated diamond surface, several molecule adsorbates such as fullerene(C_{60})[9], fluorinated variants ($C_{60}F_{48}$)[10] and solid state surface acceptors such as transition metal oxides including MoO_3[11], WO_3[12],ReO_3[13], V_2O_5[14], etc., have been developed and proven to induce diamond surface transfer doping, and the conductivity on the H-terminated diamond surface can still work at even 500℃[15]. Meanwhile, some groups have found that the carrier density in the conductive channel could be enhanced by changing the adsorbates. M Kubovic et al [16-17] systematically studied the effect of adsorbed gas NO_2 on the conductivity of H-terminated diamond. The results showed that NO_2 gas could significantly increase the hole density in the conductive channel on the H-terminated diamond surface. The hole density was up to 2.3×10^{14} cm^{-2} with 300ppm NO_2 adsorption. H Sato et al[18] compared the surface conductivity of H-terminated diamond after adsorbing NO_2 and O_3, and found that both of NO_2 and O_3 could increase the carrier density when the gas concentration increased. However, when the O_3 concentration was beyond a critical value, the carrier density would show a slight decrease, which may be due to C-H bond damage resulting from O_3. T Wade et al[19] reported that in the surface conductive channel, the carrier transport behavior could be controlled by the surface roughness. They obtained the enhanced carrier density by fabricating a rough H-terminated diamond surface in the micro scale. Thus, the diamond surface would provide more active sites to induce holes. While for the mobility, it would be limited by the surface roughness scattering. When the carrier density increased more than the carrier mobility decreased, the surface conductivity would be improved. However, until now there are few reports on the carrier mobility enhancement in the conductive channel on the H-terminated diamond surface. Generally the carrier mobility is lower than 200cm^2/Vs[7]. Generally, the carrier mobility could be improved finitely by optimizing the surface flatness and reducing the impurity level in the diamond crystal. The mobility will be suppressed by various scattering mechanisms such as the surface roughness scattering, the phonon scattering, the impurity scattering and so on[20].

In this paper, we reported that the carrier mobility on the H-terminated diamond surface could be increased to more than 300 cm^2/Vs by growing high quality epitaxial layer and mechanical cleaning. The conductivity stability was characterized, and the mobility enhancement mechanism was analyzed correspondingly.

Experimental

The work flow of preparation of the high-mobility conductive channel on the diamond surface is shown in Fig.1. Three 5mm×5mm commercial CVD single crystal diamond samples with general quality were used as the substrates. And then the high quality layers with thickness of about 100um were grown on the CVD diamond substrates by the plasma purification technology [21]. A certain amounts of O atoms were used to exhaust the nitrogen and silicon impurity atoms in the plasma environment, which could purify the diamond crystal structure. The epitaxial growth parameters of high quality diamond layers are shown in Table 1. After growth, the surface morphology of the as-grown layers were observed by optical microscopy. And then the fine polishing was conducted mechanically. The roughness (Ra) of three samples are 0.379nm, 1.1nm, 0.363nm, respectively. Three samples were cleaned in the mixed acid (volume ratio of H_2SO_4: HNO_3=5:1) at 200℃for 1h. After further cleaning in the deionized water, acetone and ethanol, respectively, they were treated by the hydrogen plasma. The hydrogen plasma treatment parameters are shown in Table.1. To avoid the chamber contamination, the chamber was cleaned by the pure hydrogen plasma for 1h before the treatment. Then the samples were put into the chamber and treated at 700℃ for 8min. After that, the surface conductivity was characterized by Hall measurement. After the Hall test, sample 1 showed the high surface resistance. Sample 2 and sample 3 were further mechanically cleaned by ultrasonic in ethanol for 15min and the surface conductivity was tested again.

The surface conductivity was tested at room temperature using HMS-3000 Hall effect testing instrument with magnetic field of 0.55T. Each sample was tested for 3 times and the average value was calculated. InVia-Reflex laser Raman spectrometer with laser wavelength of 532nm was used to obtain the PL spectra, which can show the nitrogen-related impurity information. Micro-Raman spectroscopy (JY HR-800) with laser wavelength of 514nm was used to present the crystal quality and the structures of carbon materials. Atomic force microscope (Bruker Multimode 8) was used to show the surface morphology of H-terminated diamond before and after mechanical cleaning. The scanning areas were 3μm×3μm and 10μm×10μm, respectively. Scanning electron microscope(SEM) was also used to observe the surface morphology of H-terminated diamond after the mechanical cleaning. The micro structure of diamond surface was analyzed by high resolution transmission electron microscope (HRTEM, JEM-2100F) with accelerating voltage of 200kV and point resolution of 0.25nm.

Results and discussion

After the epitaxial growth, the surface morphology of three samples tested by optical microscope are shown in Fig.2. Sample 1 shows the typical step-flow growth feature in Fig.2(a)

and Fig.2(b). While for the sample 2 and sample 3, they show the hillock growth mode in Fig.2(c-f), which is generally due to the comparatively low growth temperature. In the epitaxial growth stage, although the similar growth parameters were kept, it showed some variations on the surface morphology depending on the temperature differences. When oxygen was added in the growth environment, no obvious etching dots were found, indicating the growth rate resulting from high methane concentration is a little higher than the etching rate during the diamond epitaxial growth[22].

After the mechanical polishing, the surface conductivity of three H-terminated diamond samples was compared, as shown in Fig.3. Sample 1 shows the highest sheet resistance of 32.9kΩ/□ in Fig.3(a). Three tested values show the large dispersion. The average carrier mobility in the conductive channel is higher than 110cm^2/Vs, while the average sheet density is $1.5\times10^{12}/cm^2$. By contrast, sample 2 and sample 3 present the similar surface conductivity with sheet resistance of about 10 kΩ/□. They show the similar carrier mobility with sample 1, but the sheet concentration are much larger than that of sample 1, which cause the big difference of sheet resistance.

To further clarify the reason of surface conductivity differences, the PL spectra were tested on three samples, as shown in Fig.4. In all the spectra, the black line is the base, which is from the commercial single crystal diamond substrate. Other lines with different colors are from the epitaxial diamond layers after growth. Among three samples, besides the intrinsic diamond characteristic peak at 572nm, peaks at 575nm and 637nm appear, which correspond to the impurity $[N\text{-}V]^0$ and $[N\text{-}V]^-$, respectively. Meanwhile, the wide band between 600-800nm is considered to be related with the fluorescence of N-related impurities. For sample 1, the black line is very close to the colorful lines, indicating that the nitrogen concentration in the epitaxial layer is comparable with the substrate. While for sample 2 and sample 3, it is obvious to distinguish the grown high quality layers from the substrates. That means that, the epitaxial diamond layers of sample 2 and sample 3 are purified when using the oxygen addition in the plasma environment compared with the CVD diamond substrate. It is due to the reaction between O atoms and N atoms in the chamber and impurity N atoms will be exhausted[21-22]. Little intensity differences between the epitaxial layer and the substrate for sample 1 in the PL spectra are mainly because the epitaxial layer were almost ground off during the polishing. The low surface conductivity is mainly from the diamond substrate with high impurity concentration.

The surface morphology of sample 2 and sample 3 were observed by AFM, as shown in Fig.5. It shows many scratches on the surface of sample 2 in Fig.5(a), while sample 3 shows a very flat and smooth surface in Fig.5(b). Thus, sample 2 shows a little higher surface roughness. It is

strange that both samples show some debris with size of several hundred of nanometers on the surface. Raman spectrometer is very sensitive to the carbon materials with different structures. To check what these debris are, Raman spectra were obtained on the diamond surfaces of sample 2 and sample 3. The results are shown in Fig.6. It is clear that besides the intrinsic peak at 1332.5 cm^{-1} for diamond, an obvious peak at 1121.4cm^{-1} appear for both samples. Until now, the origin of this peak is not well understood, but it is often observed in Raman spectra of nanocrystalline diamond films[23]. Previous studies have shown that the peak at 1120 cm^{-1} usually appears for diamond nanocrystals 1-2 nm in diameter or carbon clusters of sp3 bonded material[24]. It can also be the precursor for the diamond growth[23].

To remove the debris, sample 2 and sample 3 were mechanically cleaned by the ultrasonic. The surface morphology were observed by AFM again, as shown in Fig.7. It is much clear that the debris were almost removed and the surface morphology of diamond films become much visualized. Meanwhile, the Raman spectra were tested again and the similar characteristics with Fig.6 were obtained. It indicates there is still some carbon structures on diamond surfaces although the debris were cleaned.

After mechanical cleaning, the surface conductivity of sample 2 and sample 3 were compared, as shown in Fig. 8. Each sample was tested in different three days. Both samples show stable conductivity with sheet resistance of less than 6kΩ/□. It is interesting that the carrier transport behaviors differ much for two samples. For sample 2, the carrier mobility decreases much compared with the one before the mechanical cleaning (shown in Fig.3(a)) and the carrier density increases up to $2\times10^{13}cm^{-2}$. In these days, carrier density and mobility don't change much. While for sample 3, it is surprising that the carrier mobility is higher than $300cm^2/Vs$ and the highest one is up to 365 cm^2/Vs with carrier density of 2.9×10^{12} cm^{-2} , which is also the highest value reported for the H-terminated diamond. We compared our results with those of H-terminated diamond reported by H Kawarada et al[25] and H-terminated diamond with NO_2 adsorption reported by M Kasu et al[26], as shown in Fig.9. It can be seen that H-terminated diamond with NO_2 adsorption shows higher density and less sheet resistance. While for the H-terminated diamond, the comparable resistance with the value reported by H Kawarada et al was obtained in sample 2 and sample 3. A little difference is that the high mobility contributes to the low resistance for sample 3 in our situation.

To find out the mobility enhancement mechanism, the surface morphology of sample 2 and sample 3 were further observed by SEM, as shown in Fig.10. On the surface of sample 2, it can be seen that a very thin layer is loose and will peel off from the diamond surface. While for sample 3, a smooth and flat surface is shown in Fig.10(b). To check the fine structure of the thin carbon layer,

HRTEM was used to observe the cross-section of the interface between the diamond and the thin layer. The corresponding results are shown in Fig.11. In the magnification picture shown in Fig. 11(b), on the right side is the diamond with surface orientation of (004). Based on the interplanar spacing of 0.206nm, it can be confirmed that it is the (111) crystal plane as marked. On the diamond surface, there is a thin amorphous structure with thickness of less than 10nm. Combined with the Raman results, it can be speculated that a thin amorphous carbon layer is on the diamond surface.

High surface conductivity was obtained on the H-terminated diamond layers after the hydrogen plasma treatment and mechanical cleaning. Both samples show the sheet resistance of less than 6kΩ/□. But two samples show the different carrier transport characteristics. For the sample 2 with the rough surface(roughness: 1.1nm), the carrier mobility is low and carrier concentration is relative high. While for the sample 3 with a flat and smooth surface (roughness: 0.363nm), the carrier mobility could be higher than 360cm^2/Vs. Until now it is not sure where the thin carbon layer is from, because the chamber was cleaned by H_2/O_2 mixed plasma for at least 1h before the hydrogen plasma treatment. It can be confirmed that the thin carbon layer on the diamond surface could induce the surface conductivity especially the mobility increase. This layer is less than 10nm thick. Although the fine structure of this carbon layer was not obtained, it is like nanocrystal diamond or the carbon clusters of sp3 bonded in the Raman spectra. It can't be removed by oxidizing acid boiling, showing the sp3 bond characteristics. In the view of carrier transport characteristics, the surface conductivity is still controlled by the mobility and carrier density simultaneously. Therefore, the surface conductivity is attributed to the two dimensional hole gas in the conductive channel on the H-terminated diamond. It was further confirmed because the surface conductivity would disappear if it was boiled in the oxidizing acid. For the rough surface of sample 2, the carrier mobility decreases and the carrier density increases after mechanical cleaning. In Fig.10(a) it can be seen that the thin carbon layer starts to detach from the diamond surface. More H-terminated diamond surface areas will expose in the air. The carrier density in the channel depends on the H-termination concentration on the diamond surface. More H-termination exposure may promote the carrier density increase especially for the rough surface with higher specific area[8]. For the flat surface of sample 3, the mechanical cleaning helps to remove the debris on the diamond surface, which may result in the strong surface scattering. Meanwhile, the flat surface with full coverage of the dense carbon layer promotes the carrier mobility increase drastically after the cleaning. In fact, the effect on carrier mobility in the conductive channel of H-terminated diamond may come from the surface roughness scattering, impurity scattering and the phonon scattering, and the acoustic deformation potential scattering[11]. Based on the

relationship of hole density and mobility calculated, the mobility will be limited to less than 200cm^2/Vs in the surface impurity scattering(SI) mechanism when the carrier density is 2.9$\times$10^{12} cm^{-2}, if using the ultrathin surface negative charge layer of 0.2nm. The carrier mobility we obtained is much higher than this limitation. That means the thickness of negative charge layer induced by the C-H bond will be larger in our situation. It may be due to the special transfer doping effect of H-terminated carbon layer rich in sp3 on the diamond surface. We believe that the carrier mobility could further improved by adjusting the carbon layer thickness in the carbon layer. The reason for the thin carbon layer formation and the effect of the carbon layer characteristics on the carrier mobility is still under investigation.

Conclusions

The high quality epitaxial diamond layers were obtained on the commercial CVD single crystal diamond substrates. After hydrogen plasma treatment, a thin carbon layer on the diamond was formed. It is 5-10nm thick and amorphous, as shown in HRTEM. Meanwhile, the layer with some debris contributed to the Raman peak of 1121.4 cm^{-1}, which is close to the characteristic peak of nanocrystal diamond or carbon clusters of sp3 bonded material. After the mechanical cleaning, the surface conductivity was increased dramatically. For the flat and smooth surface, the highest carrier mobility of 365 cm^2/Vs was obtained on the H-terminated diamond surface. The dense thin carbon layer promotes the high mobility by increasing the surface negative charge layer.

Acknowledgements

This work was supported by the Natural Science Foundation of Beijing, China (Grant No.4192038), National Key Research and Development Program of China (No. 2016YFE0133200) and (No.2018YFB0406501), and European Union’s Horizon 2020 Research and Innovation Staff Exchange (RISE) Scheme (No.734578).

References

[1] M Kasu. Diamond epitaxy: Basics and applications. Progress in Crystal Growth and Characterization of Materials, 2016, 62(2): 317-328.

[2] S Shikata. Single crystal diamond wafers for high power electronics. Diamond and Related Materials, 2016, 65: 168-175.

[3] J J Alcantar-Peña, E de Obaldia, P Tirado, M J Arellano-Jimenez, J E O Aguilar, J F Veyan, M J Yacaman, O Auciello. Polycrystalline diamond films with tailored micro/nanostructure/ doping for new large area film-based diamond electronics. Diamond and Related Materials, 2019, 91: 261-271.

[4] F Maier, M Riedel, B Mantel, J Ristein, L Ley. Origin of surface conductivity in diamond. Physical Review Letters, 2000, 85(16): 3472-3475.

[5] C E Nebel, B Rezek, A Zrenner. Electronic properties of the 2D-hole accumulation layer on hydrogen terminated diamond. Diamond and Related Materials, 2004, 13(11-12): 2031-2036.

[6] K G Crawford, A Tallaire, X Li, D A Macdonald, D Qi, D A J Moran. The role of hydrogen plasma power on surface roughness and carrier transport in transfer-doped H-diamond. Diamond and Related Materials, 2018, 84: 48-54.

[7] N Yang, S Yu, J V Macpherson, Y Einaga, H Zhao, G Swain, M Greg, X Jiang. Conductive diamond: synthesis, properties, and electrochemical applications. Chemical Society Reviews, 2019, 48(1): 157-204.

[8] K Hirama, H Takayanagi, S Yamauchi, J Yang, H Kawarada, H Umezawa. Spontaneous polarization model for surface orientation dependence of diamond hole accumulation layer and its transistor performance. Applied Physics Letters, 2008, 92: 112107.

[9] S Kolsch, F Fritz, M A Fenner, S Kurch, N Wöhrl, A J Mayne, G Dujardin, C Meyer. Kelvin probe force microscopy studies of the charge effects upon adsorption of carbon nanotubes and C60 fullerenes on hydrogen-terminated diamond. Journal of Applied Physics, 2018, 123: 015103.

[10] M T Edmonds, M Wanke, A Tadich, H M Vulling, K J Rietwyk, P L Sharp, C B Stark, Y Smets, A Schenk, Q H Wu, L Ley, C I Pakes. Surface transfer doping of hydrogen-terminated diamond by C60F48: Energy level scheme and doping efficiency. Journal of Chemical Physics, 2012, 136(12): 124701.

[11] Z Ren, J Zhang, J Zhang, C Zhang, S Xu, Y Li, Y Hao. Diamond field effect transistors with MoO3 gate dielectric. IEEE Electron Device Letters, 2017, 38(6): 786-789.

[12] Z Yin, M Tordjman, A Vardi, R Kalish, J A del Alamo. A diamond: H/WO3 metal–oxide–semiconductor field-effect transistor. IEEE Electron Device Letters, 2018, 39(4): 540-543.

[13] M Tordjman, K Weinfeld, R Kalish. Boosting surface charge-transfer doping efficiency and

robustness of diamond with WO3 and ReO3. Applied Physics Letters, 2017, 111: 111601.

[14] K G Crawford, L Cao, D Qi, A Tallaire, E Limiti, C Verona, A T Wee, D A Moran. Enhanced surface transfer doping of diamond by V2O5 with improved thermal stability. Applied Physics Letters, 2016, 108: 042103.

[15] J W Liu, H Oosato, B Da, T Teraji, A Kobayashi, H Fujioka, Y Koide. Operations of hydrogenated diamond metal–oxide– semiconductor field-effect transistors after annealing at 500° C. Journal of Physics D: Applied Physics, 2019, 52(31): 315104.

[16] M Kubovic, M Kasu, H Kageshima. Sorption properties of NO2 gas and its strong influence on hole concentration of H-terminated diamond surfaces. Applied Physics Letters, 2010, 96: 052101.

[17] M Kubovic, M Kasu, H Kageshima, F Maeda. Electronic and surface properties of H-terminated diamond surface affected by NO2 gas. Diamond and Related Materials, 2010, 19(7-9): 889-893.

[18]H Sato, M Kasu. Electronic properties of H-terminated diamond during NO2 and O3 adsorption and desorption. Diamond and Related Materials, 2012, 24: 99-103.

[19] T Wade, M W Geis, T H Fedynyshyn, S A Vitale, J O Varghese, D M Lennon, T A Grotjohn, R J Nemanich, M A Hollis. Effect of surface roughness and H–termination chemistry on diamond's semiconducting surface conductance. Diamond and Related Materials, 2017, 76: 79-85.

[20] Y Li, J F Zhang, G P Liu, Z Y Ren, J C Zhang, Y Hao. Mobility of two-dimensional hole gas in H-terminated diamond. Physica Status Solidi RRL, 2018, 12(3): 1700401.

[21] J L Liu, Y T Zheng, L Z Lin, Y Zhao, L X Chen, J J Wei, C M Li. Surface conductivity enhancement of H-terminated diamond based on the purified epitaxial diamond layer. Journal of Materials Science, 2018, 53(18): 13030-13041.

[22] J Liu, L Lin, Y Zheng, K An, J Wei, L Chen, L Hei, J Wang, Z Feng, C Li. Homo-epitaxial growth of single crystal diamond in the purified environment by active O atoms. Vacuum, 2018, 155: 391-397.

[23] R N Tiwari, L Chang. Growth, microstructure, and field-emission properties of synthesized diamond film on adamantane-coated silicon substrate by microwave plasma chemical vapor deposition. Journal of Applied Physics, 2010, 107: 103305.

[24] T Sharda, T Soga, T Jimbo, M Umeno. Growth of nanocrystalline diamond films by biased enhanced microwave plasma chemical vapor deposition. Diamond and Related Materials, 2001, 10(9-10): 1592-1596.

[25] H Kawarada. High-current metal oxide semiconductor field-effect transistors on H-terminated diamond surfaces and their high-frequency operation. Japanese Journal of Applied

Physics, 2012, 51: 090111.
[26] H Sato, M Kasu. Maximum hole concentration for Hydrogen-terminated diamond surfaces with various surface orientations obtained by exposure to highly concentrated NO_2. Diamond and Related Materials, 2013, 31: 47-49.

Figure captions

Fig.1 The work flow of preparation of the high-mobility conductive channel on the diamond surface

Fig.2 The surface morphology of three CVD diamond samples after epitaxial growth

(a),(b) sample 1; (c),(d) sample 2; (e),(f) sample 3

Fig.3 Surface conductivity of three H-terminated diamond samples

(a) sheet resistance; (b) carrier density and carrier mobility

Fig.4 PL spectra of three CVD diamond samples before and after epitaxial layer growth

Fig.5 Surface morphology of sample 2 and sample 3 after hydrogen plasma treatment

(a) sample 2; (b) sample 3

Fig. 6 Raman spectra of diamond surfaces after hydrogen plasma treatment

Fig.7 Surface morphology of sample 2 and sample 3 after mechanical cleaning

Fig.8 Surface conductivity of sample 2 and sample 3 tested in different three days after the mechanical cleaning

Fig. 9 Mobility vs. sheet carrier density. The corresponding results of sample 2 and sample 3 were compared with those of H-terminated diamond in reference [25] and H-terminated diamond with NO_2 adsorption in reference [26]

Fig.10 SEM photos of sample 2 (a) and sample 3 (b) on the surfaces

Fig.11 HRTEM photos of sample 3 along the cross-section direction in Fig.10(b)

(a) the cross-section of the interface between the carbon layer and diamond substrates; (b) the magnification photo of (a)

Table captions

Table 1 Epitaxial growth parameters of high quality diamond layers

Table 2 Hydrogen plasma treatment parameters

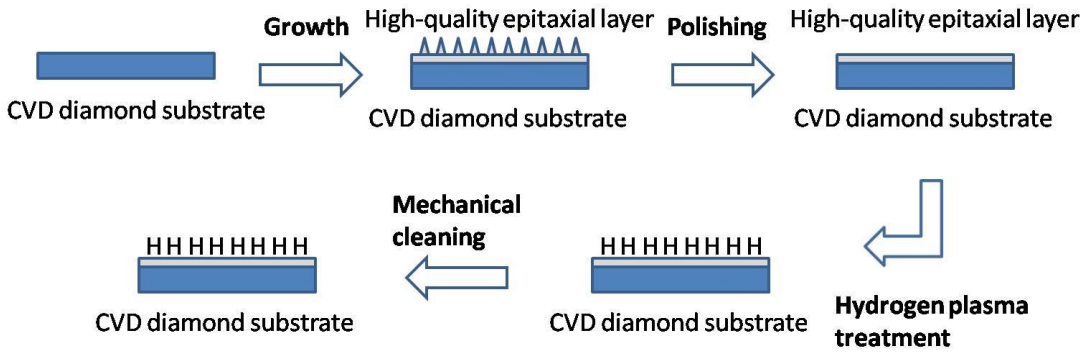

Fig.1 The work flow of preparation of the high-mobility conductive channel on the diamond surface

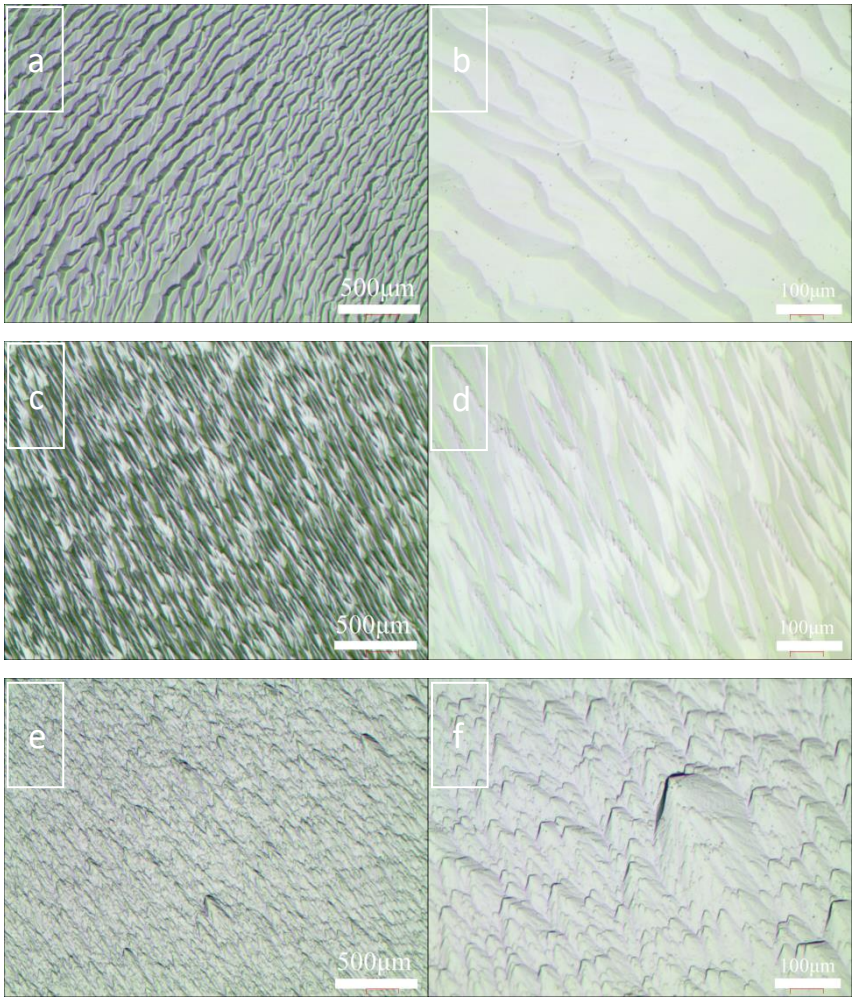

Fig.2 Surface morphology of three CVD diamond samples after epitaxial growth

(a),(b) sample 1; (c),(d) sample 2; (e),(f) sample 3

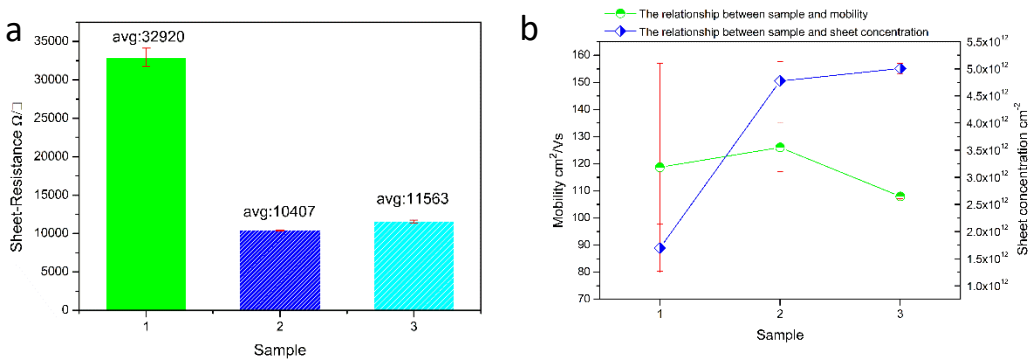

Fig.3 Surface conductivity of three H-terminated diamond samples

(a) sheet resistance; (b) carrier density and carrier mobility

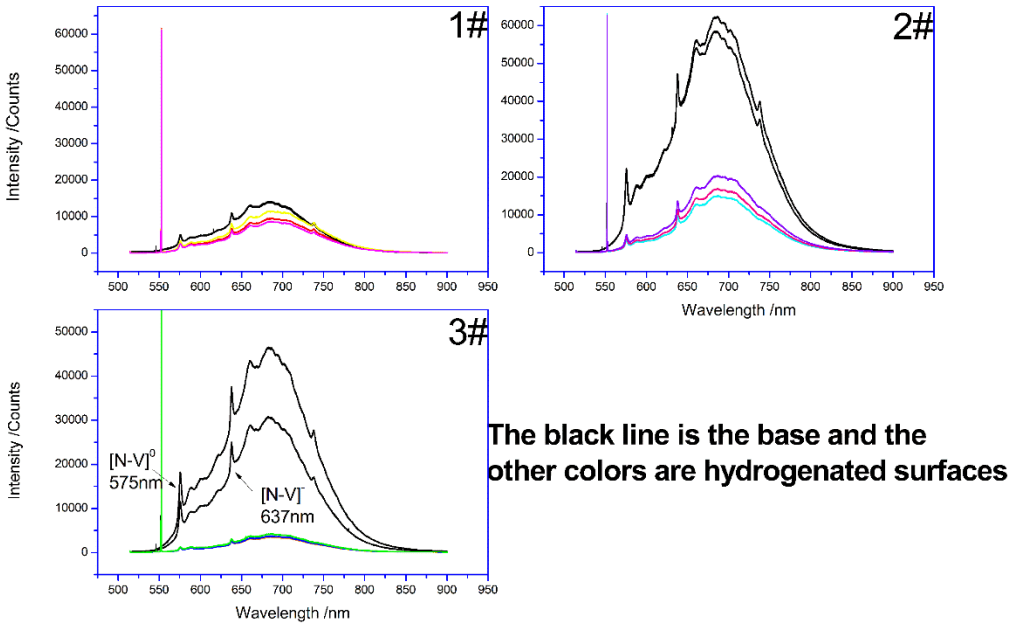

Fig.4 PL spectra of three CVD diamond samples before and after epitaxial layer growth

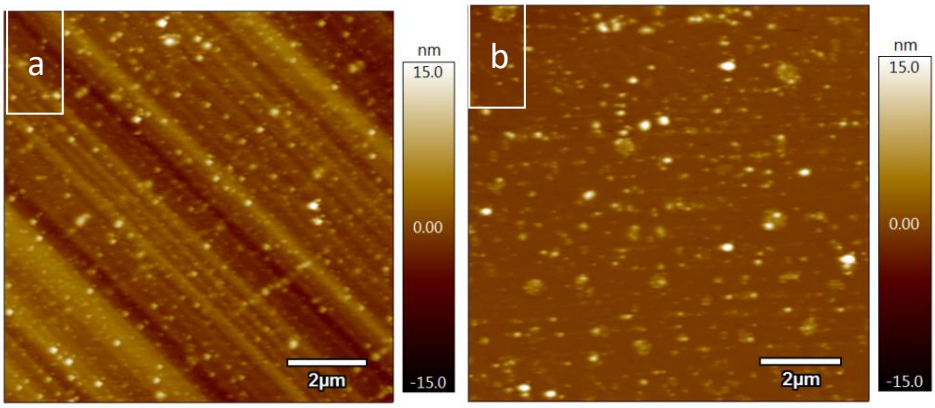

Fig.5 Surface morphology of sample 2 and sample 3 after hydrogen plasma treatment

(a) Sample 2; (b) Sample 3

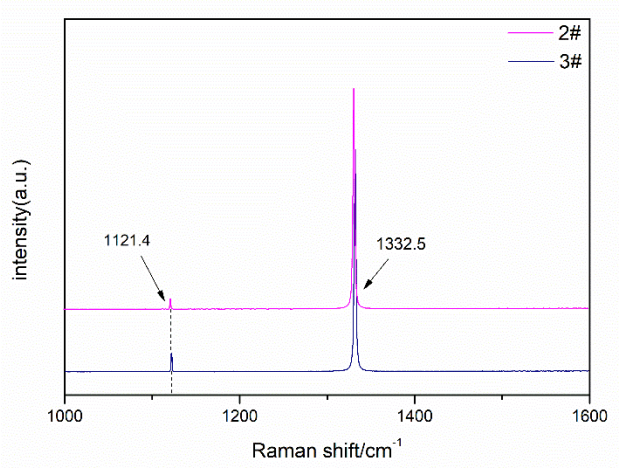

Fig. 6 Raman spectra of diamond surfaces after hydrogen plasma treatment

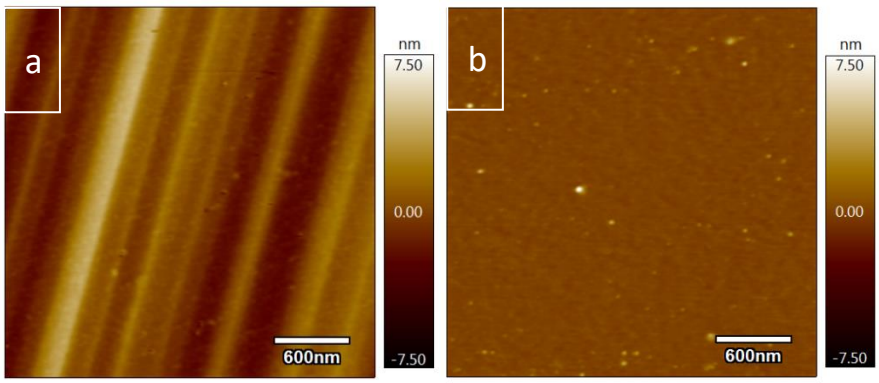

Fig.7 Surface morphology of sample 2 and sample 3 after mechanical cleaning

(a) Sample 2; (b) Sample 3

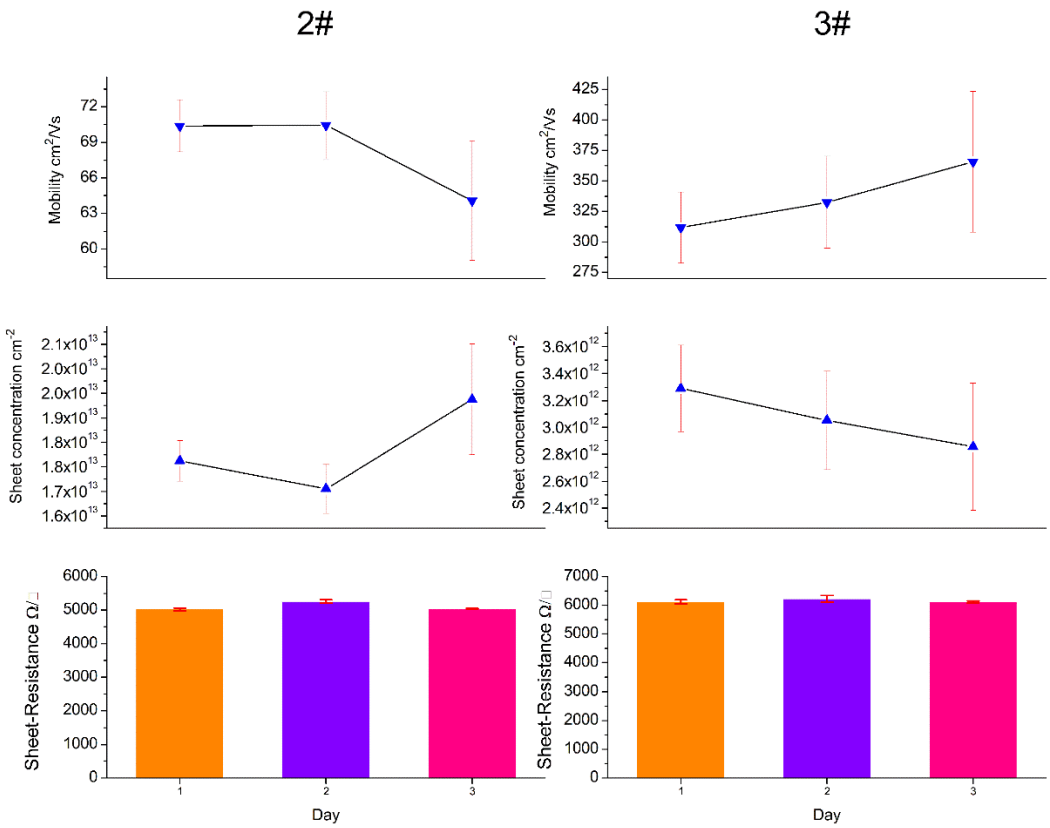

Fig. 8 Surface conductivity of sample 2 and sample 3 tested in different three days after the mechanical cleaning

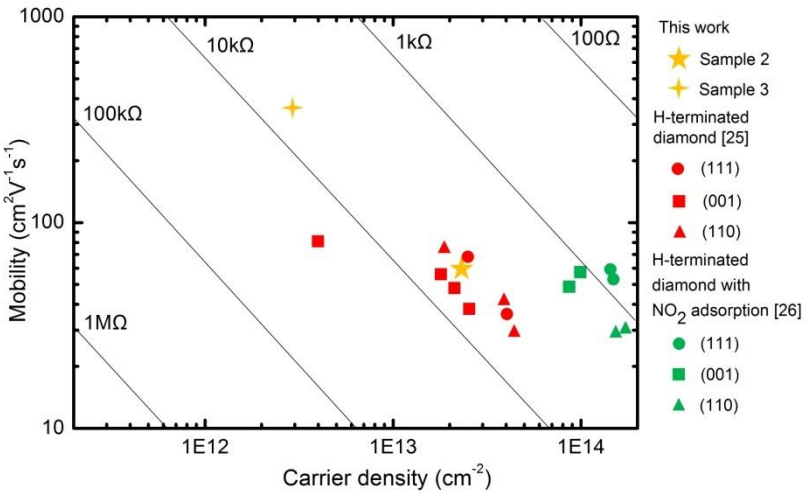

Fig. 9 Mobility vs. sheet carrier density. The corresponding results of sample 2 and sample 3 were compared with those of H-terminated diamond in reference [25] and H-terminated diamond with NO2 adsorption in reference [26]

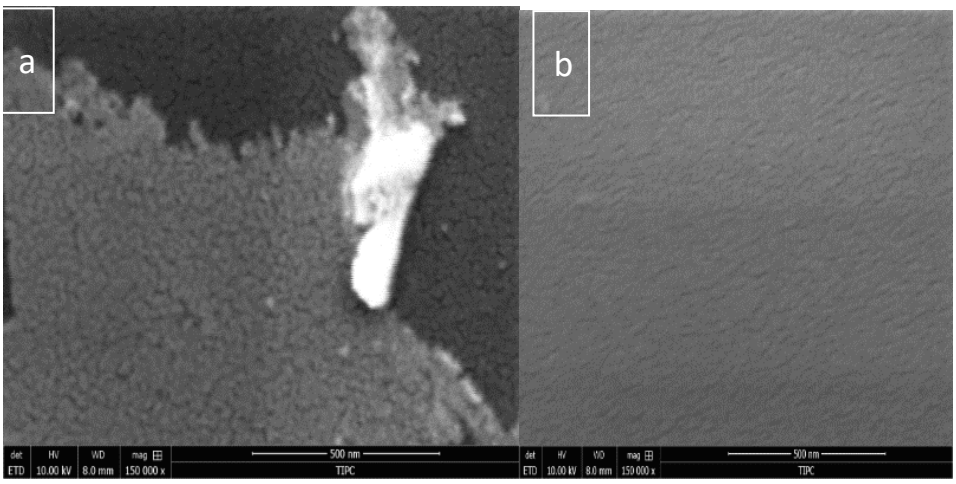

Fig.10 SEM photos of sample 2 (a) and sample 3 (b) on the surfaces

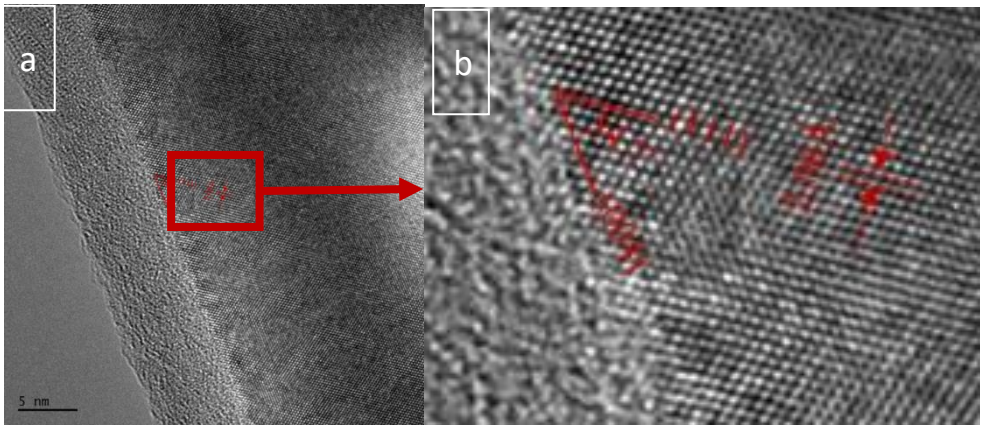

Fig.11 HRTEM photos of sample 3 along the cross-section direction in Fig.10(b)

(a) the cross-section of the interface between the carbon layer and diamond substrates;

(b) the magnification photo of (a)

Table 1 Epitaxial growth parameters of high quality diamond layers

Sample	Temperature/℃	CH_4 concentration/%	O_2 concentration/%	Duration/h
1, 2, 3	800~900	3-5	0.3-0.7	24

Table 2 Hydrogen plasma treatment parameters

Temperature/℃	Power/W	Pressure/kPa	Duration/min
690~700	1100	5.55	8